Unsaturated flow through a fracture–matrix network: Dynamic preferential pathways in mesoscale laboratory experiments

R. J. Glass,[1] M. J. Nicholl,[2] S. E. Pringle,[1] and T. R. Wood[3]

Received 9 October 2001; revised 7 June 2002; accepted 7 June 2002; published 7 December 2002.

[1] We conducted two laboratory experiments at the meter scale in which water was applied to the top of an initially dry, uncemented wall composed of porous bricks. One experiment (Experiment 1) encouraged evaporation and resulting mineral precipitation, while the other (Experiment 2) was designed to minimize these processes. In both cases, processes acting within the fracture network controlled early time behavior, forming discrete pathways and demonstrating fractures to act as both flow conductors and capillary barriers. At a later time, evaporation–mineral precipitation in Experiment 1 constrained flow, strengthening some pathways and starving others. In Experiment 2, the wetted structure took on the appearance of a diffuse plume; however, individual pathways persisted within the wetted structure and interacted, displaying erratic outflow over a wide range of timescales, including switching between pathways. Thus, under conditions of constant supply and both with and without evaporation–mineral precipitation, unsaturated flow through fractured rock can create dynamic preferential pathways. *INDEX TERMS:* 1829 Hydrology: Groundwater hydrology; 1875 Hydrology: Unsaturated zone; 1832 Hydrology: Groundwater transport; *KEYWORDS:* preferential flow, fracture network, vadose zone, unsaturated flow

Citation: Glass, R. J., M. J. Nicholl, S. E. Pringle, and T. R. Wood, Unsaturated flow through a fracture–matrix network: Dynamic preferential pathways in mesoscale laboratory experiments, *Water Resour. Res.*, *38*(12), 1281, doi:10.1029/2001WR001002, 2002.

1. Introduction

[2] Over the past 10 years, a number of laboratory investigations have considered the physics of unsaturated flow both within discrete fractures, and between a fracture and the adjacent matrix. In doing so, these investigations have uncovered a number of fundamental physical processes that strongly influence behavior at the scale considered. Many of these processes (e.g., gravity-driven fingering, phase entrapment, phase interference) create flow structures that are not only dependent on initial and boundary conditions, but also vary in time [e.g., *Glass et al.*, 2001]. In order to correctly incorporate these processes into conceptual models applicable to the field, we must first understand how processes at the local scale (i.e., a single fracture or single fracture–matrix system) couple to determine behavior at larger scale (i.e., fracture–matrix network).

[3] In earlier work, *Glass et al.* [1995, 1996] suggested that most local processes enhanced the critical influence of the fractures to both conduct and focus flow, as well as to effectively decouple the intervening matrix. Considering larger scale behavior within the fracture–matrix network, they hypothesized that gravity-driven fingers within steeply dipping fractures would converge at capillary barriers created by subhorizontal fractures. The resulting flow convergence with depth would eventually lead to the formation of large scale pathways, even in the absence of significant vertical heterogeneities (e.g., major faults). Around these pathways, steeply dipping fractures would act as capillary barriers to lateral flow between adjacent matrix blocks, and hence keep the pathway slender with depth. Once formed, pathways may be insensitive to some system perturbations (e.g., annual weather patterns), but likely move under others (e.g., climate change, changes in stress-strain field due to tectonic activity). Over time, geochemical activity along a pathway could also alter system properties sufficiently to secure the continued persistence or the extinction of that pathway.

[4] The behavior hypothesized by *Glass et al.* [1995, 1996] is consistent with field observations that suggest large scale preferential flow. Focused transport pathways are a common occurrence in unsaturated fractured rock [e.g., *Russell et al.*, 1987]. There is also a variety of field evidence that shows rapid and deep penetration in fractured vadose zones by meteoric water [e.g., *Fabryka-Martin et al.*, 1996; *Davidson et al.*, 1998], as well as from ponded infiltration experiments [e.g., *Glass et al.*, 2002]. However, field observations alone are insufficient to test the hypothesized causes and subsequent behavior of large scale preferential pathways. Instead, mesoscale experiments (~one to several meters) are required where critical system parameters can be controlled and varied so that network scale behavior may be understood systematically.

[5] In this paper, we present the results of two mesoscale (~1 × 2 m) experiments designed to demonstrate the coupling between single fracture and single fracture–matrix behavior within a fracture–matrix network. We designed the first experiment to cause evaporation and subsequent

[1]Flow Visualization and Processes Laboratory, Geohydrology Department, Sandia National Laboratories, Albuquerque, New Mexico, USA.
[2]Department of Materials, Metallurgical, Mining, and Geological Engineering, University of Idaho, Moscow, Idaho, USA.
[3]Idaho National Engineering and Environmental Laboratory, Idaho Falls, Idaho, USA.

0043-1397/02/2001WR001002$09.00

mineral precipitation processes to become dominant with time, while these processes were minimized for the second experiment. Results of both experiments clearly demonstrate the ability of processes acting on, and within a fracture–matrix network to create distinct pathways through the system. In addition, we discover that despite steady supply, these pathways are dynamic in both time and space.

2. Experimental System and Design

[6] Our experimental system consisted of precast concrete bricks stacked within a simple load frame to form an uncemented brick wall (Figure 1) 5.7 cm thick, 98 cm wide, and either 171 cm (Experiment 1) or 228 cm (Experiment 2) tall. In order to maximize matrix interaction, we chose the most porous bricks available from a local building supply. The type of brick selected is known locally as "Gray Scoria Brick", and has dimensions of $19.0 \times 8.9 \times 5.7$ cm. Measurements on core samples taken from three typical bricks yielded a porosity of 0.35, saturated conductivity of 1.8×10^{-4} cm/sec (falling head method) and pressure–saturation relation for drainage as shown in Figure 2 (UFA centrifuge method [*Conca and Wright*, 1997]). Our preparation of the bricks included scraping off surface protrusions that were artifacts of the casting process, thus leading to "tight" fractures when the air dried bricks were stacked in horizontal rows within the load frame. In order to assure good contact between adjacent bricks, a horizontal compressive force was applied to each row. To characterize the gross aperture field within the network, a feeler gage was inserted into and along fractures. Between 25–75% of every fracture was below 0.038 mm (the smallest gage) and considered to be contact area between the bricks. In general, maximum values in each fracture occurred near the fracture edge and ranged from 0.05 mm up to 0.2 mm, however several locations within the field had values as high as 0.5 mm. Fracture intersections, where the corners of four bricks came together, formed larger gaps in the range of 0.5 to 3 mm due to the imperfect mating of often chipped brick corners. A peristaltic pump was used to supply water to the network through a needle inserted into the top of vertical fracture V5 (see Figure 1). Supply to the network was monitored by placing the inflow reservoir on an electronic balance (0.1 g resolution). Imbibition of water darkened the light colored bricks, allowing us to document temporal development of the unsaturated flow field with photographs.

[7] Our first experiment (Experiment 1) was designed to consider pathway evolution in the presence of evaporation and the resulting mineral precipitation, while the second (Experiment 2) was designed to minimize the influence of these same processes. For Experiment 1, we used water equilibrated to the media (final pH ~10, filtered) and made no effort to restrict evaporation from the wall. Based on bench scale tests with pairs of bricks, we selected a flow rate of 1.2 ml/min for Experiment 1. For Experiment 2, we enclosed the entire experiment with clear plastic panels (see Figure 1b). The enclosure was shaped like an A-frame, with a footprint of $\sim 1.2 \times 1.2$ m and internal volume of ~3 m^3; we added a small hole at the top for fluid supply, and a side hatch to allow access for maintenance. Tests showed that while acting as a diffusional barrier, gas pressure equilibrated within minutes across the enclosure. To reduce geochemical activity in Experiment 2, we leached easily dissolved minerals from the bricks prior to the experiment. First we submerged the bricks in deionized (DI) water for five days, changing the water daily. We then lashed the bricks into a modified laundry machine and agitated them in warm DI water (~52°C); following the spin cycle, remaining water was removed through forced hot air convection. As a compromise between DI (strong solvent) and chemically equilibrated water (high TDS), we used local tap water (rich in the bicarbonate ion) for the infiltrating fluid. As evaporative losses from Experiment 1 were on the order of 0.2 ml/min, we set the flow rate for Experiment 2 at 1ml/min.

[8] In addition to minimizing evaporation and precipitation, the design for Experiment 2 also included a number of refinements based on our experience during Experiment 1. We note that none of these refinements altered the fundamental character of the experiment, thus allowing direct comparison between Experiments 1 and 2. In order to maximize opportunities for flow structure development, we raised the height of our second brick wall from 9 to 12 rows of bricks (12 rows was the maximum allowed by room height). Also, in Experiment 1, the bottom of the wall acted as a capillary barrier. To create a free-flowing boundary for Experiment 2, we installed fiberglass wicks at the bottom of each vertical fracture, with a length of ~19 cm (1 brick). Outflow and inflow measurement was monitored manually in Experiment 1, while for Experiment 2 it was automatically monitored at 5 min intervals.

[9] Finally, because we monitored outflow automatically in Experiment 2, we discovered unsteady outflow behavior. To investigate this behavior, we extended the duration of the experiment and implemented a series of modifications intended to both reduce, and study the unsteady behavior. Approximately 1400 hours after starting flow, we constructed an outer enclosure surrounding the experiment; this modification was designed to reduce temperature and humidity gradients across the enclosure boundaries, particularly during maintenance. At ~2500 hours, we expanded our outflow measurements from one reservoir collating all ten fracture outputs, to five reservoirs, each collecting outflow from two adjacent fractures. Between ~3600 and ~6800 hours, we installed sensor arrays to monitor temperature and liquid water tension within matrix blocks, as well as water vapor tension within the experimental enclosure. Time lines for both Experiment 1 and Experiment 2 are given in Table 1.

3. Experiment 1: Active Evaporation and Mineral Precipitation

[10] A time history of the developing wetted structure within the fracture–matrix network over the first 225 hours of Experiment 1 is displayed in Figures 3a and 3b. Water reached the bottom of the wall 47.5 hours after we started flow, following a pathway that not only included both fractures and matrix, but also behaved erratically in time, with a "stop and go" nature that was indicative of fracture intersections performing as capillary barriers. Water moved rapidly downward from the supply point within the fracture (V5), passed through the first fracture intersection (H1), and on to the second (2 hours). At this intersection, the flow path turned to the right within a horizontal fracture (H2), and then once again continued downward (V6) to the next intersection (4 hours), producing a lateral offset in the

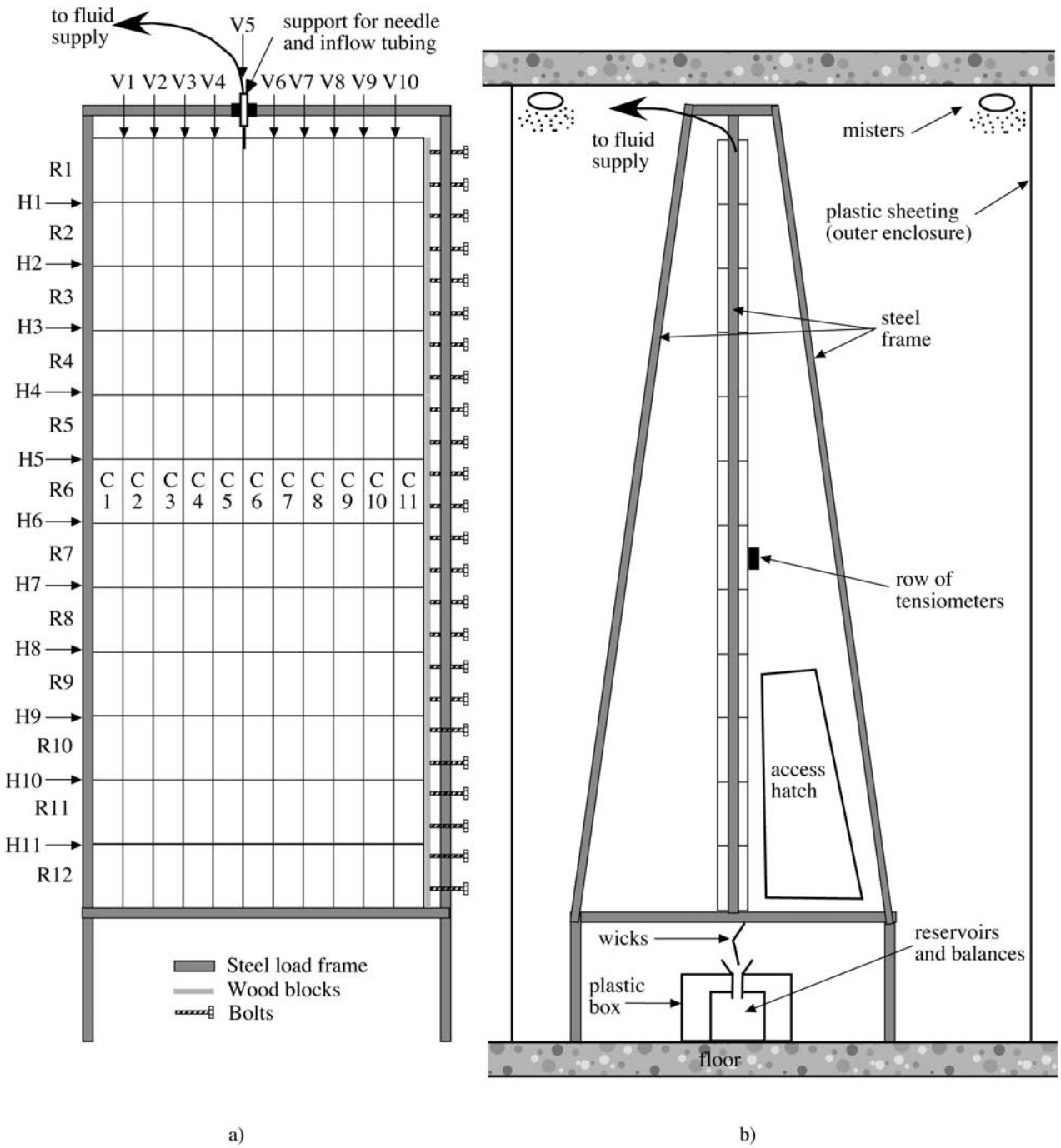

Figure 1. Schematic of experimental system: a) Front view. Bricks and fractures are numbered from the upper left hand corner; V and H represent vertical and horizontal fractures respectively, while C and R represent column and row for the bricks themselves. Machine bolts along the right-hand edge of the load frame were used to apply force to individual wood blocks placed at the end of each row of bricks, thus placing the row under a horizontal compressive stress. Bricks were stacked with the largest face (19.0 × 8.9 cm) exposed, and the longest length (19.0 cm) oriented vertically. Note that Experiment 1 was 9 bricks high (rows were numbered 1–9), while Experiment 2 had 12 rows of bricks as shown here; both were 11 bricks wide. b) Side view. The steel frame was in place for both experiments, other features were added for Experiment 2 (see time line in Table 1). The experimental enclosure was formed by bolting and sealing clear plastic panels to the steel frame used for Experiment 1. Between 1400 and 2500 hours after starting flow in Experiment 2, we added the outer enclosure, misters, and revised the outflow reservoirs, including the plastic box to protect the balances from humidity. At ~3600 hours in Experiment 2, we began installing tensiometers and thermocouples (not shown).

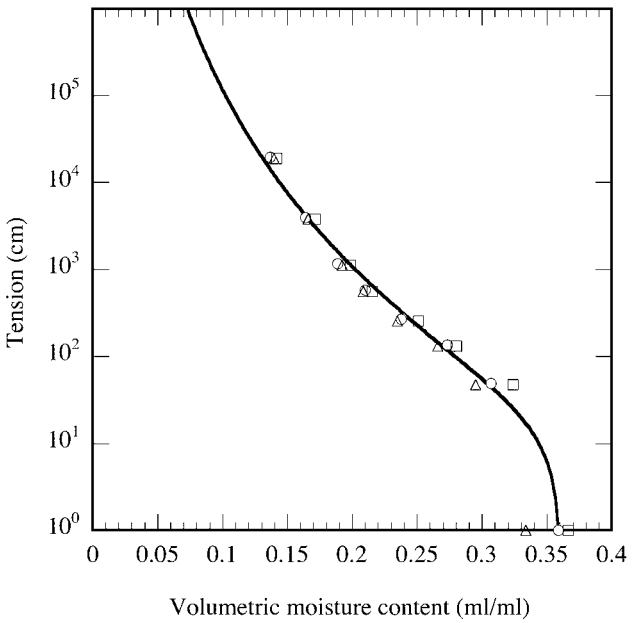

Figure 2. Capillary properties for the Gray Scoria Brick: Capillary tension head is plotted as a function of moisture content for three samples. Data was collected for drainage using a centrifuge method [*Conca and Wright*, 1997]. The van Genuchten relation (solid line) was fit to the combined data to yield parameter values for the inverse capillary length, α (0.049 cm^{-1}), and pore size distribution, n (1.148), with an R^2 of 0.994.

pathway. After another turn to the right (H3), matrix flow into the brick below (C7R4) dominated growth in this "primary" pathway (8.5 hours). The primary pathway continued as matrix flow, with the block (C7R4) wetting downward to the next horizontal fracture (H4). When fracture H4 was crossed (14.5 hours), flow moved downward in the fracture to the right (V7). This mixture of flow primarily in fractures, with some intervening stretches in matrix (brick C8R8) continued to the bottom of the network (47.5 hours). Meanwhile, starting at ~8 hours, a "secondary" pathway began to slowly grow down to the left of the primary, emanating from within the supply fracture (V5) where the first right turn (H2) in the primary had occurred. Once again, this secondary pathway included mainly fracture flow, with some segments of matrix flow (bricks C6R6 and C6R7). The secondary pathway remained clearly separate from the primary pathway, eventually reaching the bottom of the network at ~216 hours.

[11] The absorption of water from fractures into adjoining bricks is seen throughout this initial period. However, when the wetting front within the matrix reached the far side of a brick, the next fracture tended to form a capillary barrier, slowing lateral advance (e.g., see the wetting of bricks in columns 5 and 6, rows 1 and 2 from the central supply in fracture V5). In addition, when flow occurred primarily downward within a brick, the fracture on either side also constrained flow (e.g., see the wetting of bricks C7R4 and C8R8 in the primary pathway and C6R6 and C6R7 in the secondary pathway). This influence of fractures as both vertical and horizontal capillary barriers imparted a blocky nature to the wetted structure, and tended to constrain flow in each pathway to a narrow zone, approximately two bricks wide. At 225 hours, the wetted structure had developed to be nearly filled in and looked as a narrow plume 2 bricks wide (1 fracture) in the top two rows, and 4 bricks wide (3 fractures) below. However, considering the growth history and the manner in which water pooled at the bottom boundary of the network, it was obvious that this plume was composed of two distinct pathways that diverged below the second row of bricks. It was also obvious that the primary pathway continued to carry most of the flow though the network. Additionally, we visually observed low frequency pulsation of aperture spanning flow within two of the vertical fractures along the primary pathway (the gap between bricks was sufficiently large at these locations to see light through the fracture). Since pulsation is a hallmark of gravity-driven fingering [e.g., *Nicholl et al.*, 1993; *Glass and Nicholl*, 1996; *Su et al.*, 1999], the tight fracture network within a permeable matrix obviously did not preclude gravity-destabilized flows.

[12] After 225 hours into the test (Figure 3c), we began to observe a series of changes in the wetted structure (and thus the corresponding flow field). First, we noted the buildup of precipitate along the face of the wall in a series of downward flowing fingers (all ~0.5 cm wide) that sometimes continued across horizontal fractures (usually with a shift). Close examination of the brick faces showed fingered film flow at these locations, but not between; evaporation of the equilibrated water from flowing fingers was precipitating calcium carbonate on the surface of the bricks. Second, we began to see the buildup of precipitate along the edges of the gross wetted structure, presumably not only on the brick faces, but also within the matrix. Third, temporal changes in coloration (darkness) over the lower portion of the wetted structure indicated that the flow pathways were shifting. We followed these developments up until 936 hours (see Figure 3d). During this period, the bottom quarter of the primary pathway was slowly starved and eventually eliminated by evaporation. In addition, the entire wetted structure narrowed, and at the bottom, a single fracture (V5) with wetted bricks on either side carried all the flow. Buildup of precipitate around the pathway suggests the possibility of sealing the matrix against further evaporation, thus "armoring" the pathway and assuring its persistence as suggested by *Glass et al.* [1995, 1996].

Table 1. Experimental Time Lines

	Experiment 1
47.5 hours	Water reached bottom (171 cm)
225 hours	Noticeable carbonate precipitation began
936 hours	Reduced evaporation rate with draped plastic
1704 hours	Experiment terminated
	Experiment 2
130 hours	Water reached bottom (228 cm)
240–264 hours	Inflow interrupted
412–440 hours	Inflow interrupted
~1400 hours	Outer enclosure built to reduce humidity gradients
~2500 hours	Single outflow expanded to monitor paired fractures
~3600–6800 hours	Temperature and pressure sensor arrays installed and debugged
~10,100–10,500 hours	Inflow pump turned off
10,795 hours	Experiment terminated

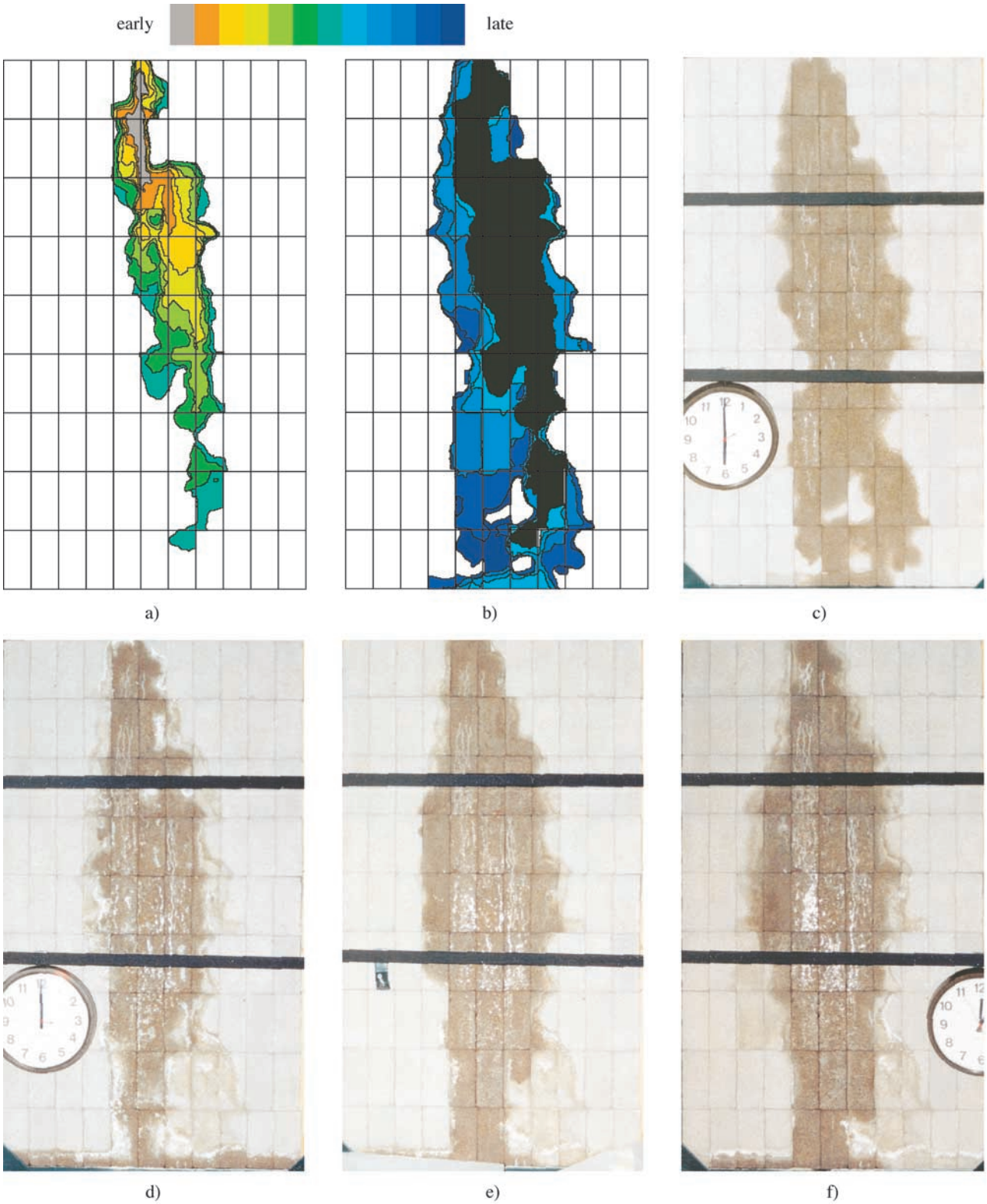

Figure 3. Experiment 1 wetted structure development and carbonate precipitation: a) Individual colors represent extent of the wetted structure at 2, 4, 8.5,14.5, 20, 30, 42 hours. b) Continued development of the flow field, region shown in black represents the time span covered in a); remaining colors show wetted structure development at 52.5, 95.5, 149.5, 201.5, 225.5 hours. Additional photographs show the wetted structure at c) 225 hours, d) 936 hours, e) 960 hours, and f) 1704 hours. White regions are calcium carbonate, some of which has been precipitated from surface film flow in narrow fingers.

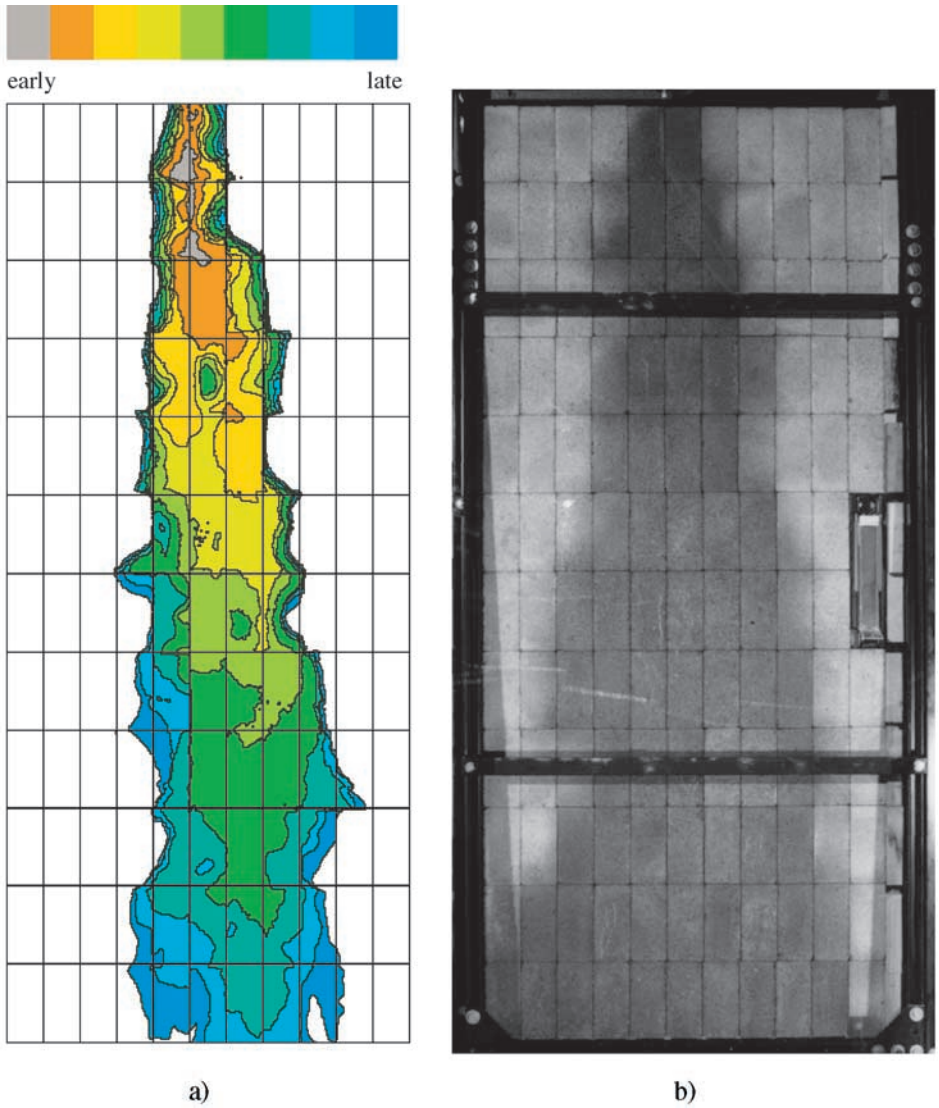

Figure 4. Experiment 2 wetted structure development and long time diffuse plume: a) Individual colors represent extent of the wetted structure at 3, 11, 25, 44, 65, 95, 123, 144, and 177 hours. b) Photograph showing diffuse plume structure at ~1400 hours.

[13] With Experiment 1 having run its intended course, after 936 hours we covered the experiment with plastic sheet to see if a reduction in evaporation would now significantly alter the flow field. Over the course of the next day, some of the precipitate on the wall face appeared to dissolve, and we found the wetted structure to expand back to near it's extent at 225 hours (Figure 3e). However, the starved primary pathway at the bottom right was not reinstated. We did find that between 960 and 1104 hours, a new "tertiary" pathway grew downward along the left side of the wetted structure (columns 3 and 4 from rows 6 to 7), which then stopped and was subsequently erased by evaporation between 1104 and 1272 hours. Vestiges of this zone can be seen in the final photograph at 1704 hours (Figure 3f). In addition, another tertiary pathway began growth along the right side in column 7, row 8. This particular zone had remained dry during the initial wetting through 225 hours, separating the original primary and secondary pathways. After 1704 hours, we terminated Experiment 1. A postmortem showed that substantial calcium carbonate precipitation was restricted to the evaporative surfaces of the experimental wall, with little to no precipitation within the fractures of the main pathway through the network.

4. Experiment 2: Minimized Evaporation and Mineral Precipitation

[14] A composite image showing development of the wetted structure for Experiment 2 is presented as Figure 4a. Water moved down fracture V5 to the third intersection (H3), and then turned to the right. The pathway split on either side of brick C5R4, with the left-hand path advancing slightly slower than the right. From there on, the paths seem to coalesce and we see more matrix participation than in the first experiment, which could have resulted from reduced evaporation, dissimilar preparation of the bricks, or slight differences in the assembly of the wall. It is important to note that despite this increased matrix interaction, the rapid

wetting of individual fractures with pauses at fracture intersections as well as the overall blocky wetted structure within the matrix was similar to Experiment 1, once again emphasizing the importance of fractures and fracture intersections as capillary barriers.

[15] Considering the 33% increase in system height and 20% decrease in flow rate from Experiment 1, we anticipated that the wetted structure would contact the bottom boundary after ~76 hours; not only did it require 130 hours, the resulting structure was visually more uniform than observed in Experiment 1. From 130 to 200 hours, wetted structure in the two bottom rows grew to a width of 5 bricks; growth occurred from above (not laterally) by flow through both the matrix and vertical fractures. After 200 hours, the structure continued to slowly widen and, near the close of this initial period (1364 hours), wetted structure (Figure 4b) resembles what one might expect from a steady state solution of a porous continuum model; however, as documented below, flow through the fracture–matrix network was neither steady nor uniformly distributed, as might be predicted by such a continuum representation.

[16] We began monitoring outflow shortly after water started to drip from several of the wicks. Over the next ~12 days, we alternated between monitoring combined outflow from all fractures, and outflow from the most active fracture (V6); both increased gradually, but not smoothly, with numerous short periods (minutes to hours) where outflow rate actually declined. The inflow pump malfunctioned twice during this period (see Table 1); these were the only interruptions of the inflow during Experiment 2 until its final days ~15 months later. For the second pump failure, outflow had essentially stopped when inflow was restarted. Data from this second restart (Figure 5a) shows a 4.9 hour lag between inflow initiation and first measured outflow, followed by a generally smooth increase in total outflow rate.

[17] During the ~240 hr period after the second restart, total outflow rate slowly rose to ~0.9 ml/min; in doing so it displayed a rich temporal structure not present in the inflow (see Figure 5b). We also noticed that opening the hatch for maintenance, even for a 2–3 minute period, caused a rapid and significant decrease (~40%) in outflow rate, with recovery requiring ~2.5 hours. Figure 5c shows inflow and outflow data for the period 1030 to 1270 hours after outflow had reached a near long-term average of 0.885 ml/min. After removal of the inconsistent data points (e.g., maintenance intervals), variance of the outflow (σ^2 = 0.0023 cm^2/min^2) during this period was over an order of magnitude greater than that of the inflow (σ^2 = 0.00017 cm^2/min^2). While the variation in the inflow can be associated with 0.1g balance resolution, outflow data displays both a higher degree of random variation and a strong periodicity. The dominant periodic cycles are at ~12 and 24 hours, with a combined amplitude of ~0.1–0.15 ml/min (10–20%). There are also variations (trends) at the scale of the data set.

4.1. System Modifications (~1400 to ~2500 Hours)

[18] Beginning at ~1400 hours, we implemented a suite of modifications designed to help us understand system behavior, as well as possibly calm its unsteady nature (i.e., further reduce external perturbations). In order to further reduce evaporative losses to the relatively dry laboratory environment, we first surrounded the experimental enclosure with a humidity barrier. An outer enclosure was constructed from thick plastic sheet, and a humid environment was maintained by continually misting water at the top (see Figure 1b). A positive side effect of adding the outer enclosure was additional isolation from external thermal perturbations; unfortunately, it also prevented us from collecting additional photographic records of the wetted structure. We then reconfigured the outflow reservoirs to obtain continuous measurements from paired fractures (V1&V2, V3&V4,...V9&V10). Each set of adjacent wicks was directed to a funnel glued to the top of a box containing the reservoirs and electronic balances; the reservoirs were emptied remotely, using an external pump. This arrangement for transferring fluid to the measurement system (see Figure 1b) was designed to minimize evaporative loss, while isolating the balances from high humidity within the experimental enclosure.

4.2. Expanded Outflow Data (Beginning ~2500 Hours)

[19] Figure 6 shows inflow and outflow rates over two typical 50 hour sequences separated by a gap of ~4 days. We found variance of the total outflow to decrease by more than 35% with respect to earlier measurements (Figure 5c), suggesting that the outer enclosure and humidity barrier had significantly reduced the influence of external perturbations. It appears that much of the reduction in outflow variance can be attributed to damping of the diurnal cycle, which while still present, is of reduced magnitude; the 12 hour cycle appears to have been damped to a lesser degree. We also noted that variance of the total outflow is less than the sum of the variances for the individual outflows, suggesting a negative correlation between flows from adjacent fracture pairs. Correlation coefficients (C_c) for the data in Figure 6 shows strong negative correlations between the outflows from fracture pairs 5–6 and 7–8 (C_c = −0.5 and −0.28 for the data shown in Figures 6a and 6b, respectively). Examples of negative correlation between the outflows of these adjacent fracture pairs can be clearly seen in Figure 6. In particular, an abrupt increase in outflow from fractures 7–8 at 2619 hours coincides with a slightly less abrupt decrease from fractures 5–6. This behavior suggests that flow has switched between two well defined pathways within the fracture–matrix network. More gradual switching between these same fracture pairs can be seen at 2645 and 2774 hours; because we combined outflows from adjacent fractures, additional path switching may have gone unnoticed.

[20] Between the two time periods shown in Figure 6, average inflow increased by ~1.5% (0.976 to 0.991 ml/min), likely due to changes in line voltage. During that same time, outflow rates from all fractures have changed, with 5–6 and 7–8 (less so) increasing at the expense of 3–4 and 1–2 (less so). Thus, for this particular time period, outflow has become more focused, despite slightly increased inflow. Finally, in Figure 6a, most of the low frequency information from individual fracture pairs may be attributed to path switching (negative correlation), while in Figure 6b, the low frequency information contains both negatively and positively correlated changes. As a result, the total outflow for the period shown in Figure 6a shows

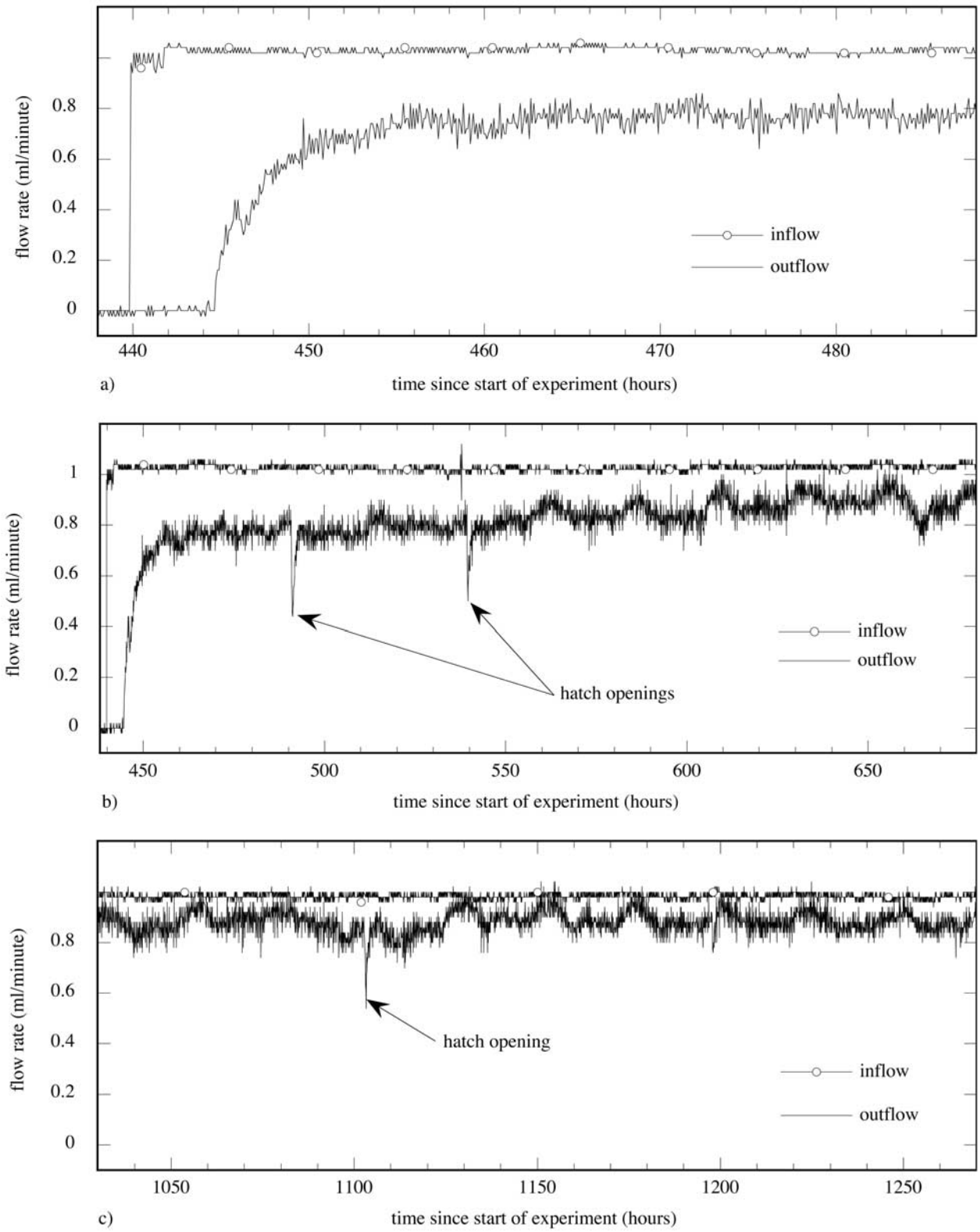

Figure 5. System response after being restarted following the second pump failure: Inflow rates are shown for a) 435–485 hours; b) 430–670 hours; and c) 1030–1270 hours. Note that inflow rate decreased slightly (~4.1%) between 670 and 1030 hours due to adjustment of the pump to keep inflow rate near to 1.0 ml/min.

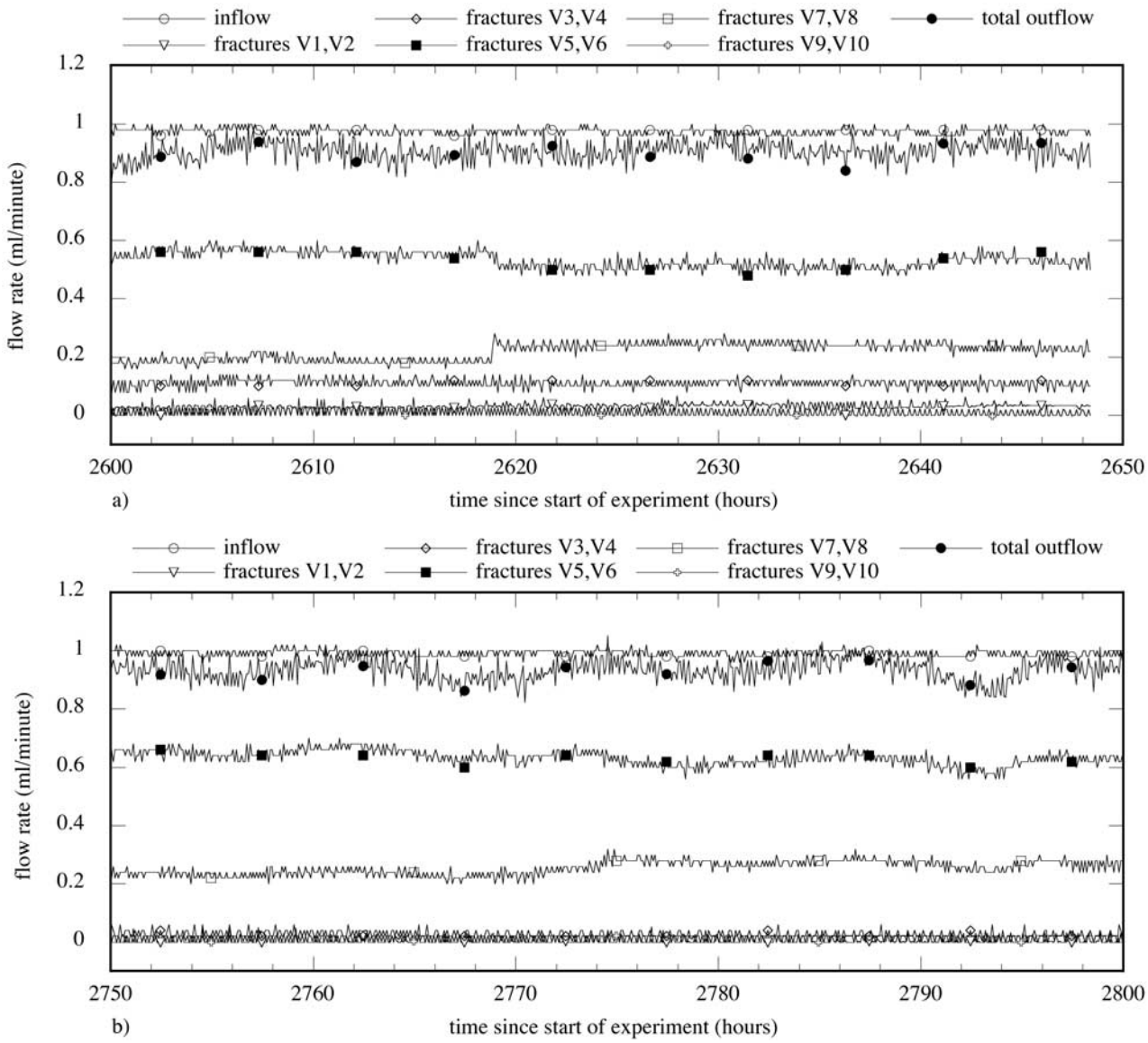

Figure 6. Expanded outflow data for typical 50 hour periods separated by ~4 days: a) 2600–2650 hours variance of total outflow rate = 0.0015 cm^2/min^2, variance of the total outflow is ~32% less than the sum of the individual variances. b) 2750–2800 hours variance of total outflow rate = 0.0014 cm^2/min^2, variance of the total outflow is ~18% less than the sum of the variances from the contributing fracture pairs.

less low frequency information (i.e., changes cancel out) than the period shown in Figure 6b.

4.3. Sensor Array Implementation (~3600 to ~6800 Hours)

[21] To better characterize both the continued fluctuations and the presumed quiet laboratory environment, from ~3600 to ~6800 hours, we implemented and debugged a tensiometer and thermocouple array. At ~3600 hours, we installed 5 tensiometers along the centerline of row 6, and within the core of the diffuse plume. Tensiometers were fabricated by cementing 7 mm diameter discs of porous metal into modified Swagelok™ fittings; clear rigid tubing was used to support a water column connecting each tensiometer to individual pressure transducers located outside the experimental enclosures. Tensiometers were pressed up against the faces of individual bricks (see Figure 1b) with hydraulic contact provided via filter paper. At ~6200 hours, a thermocouple array was added; 16 thermocouples were positioned at various locations within the experimental enclosure, outer enclosure, and surrounding laboratory. At ~6800 hours, the tensiometer transect was extended to the edges of brick wall to yield a total of 15. At the same time, we also installed 6 additional tensiometers to record oscillations in vapor tension within the enclosure; these were placed at the same height as those on the wall, but without hydraulic contact to the bricks. All thermocouples and transducers were monitored at 5 min intervals.

4.4. Tension and Temperature Data (Beginning ~6000 Hours)

[22] In general, tensiometers in the middle of the transect (within the flow field) showed near zero tensions from

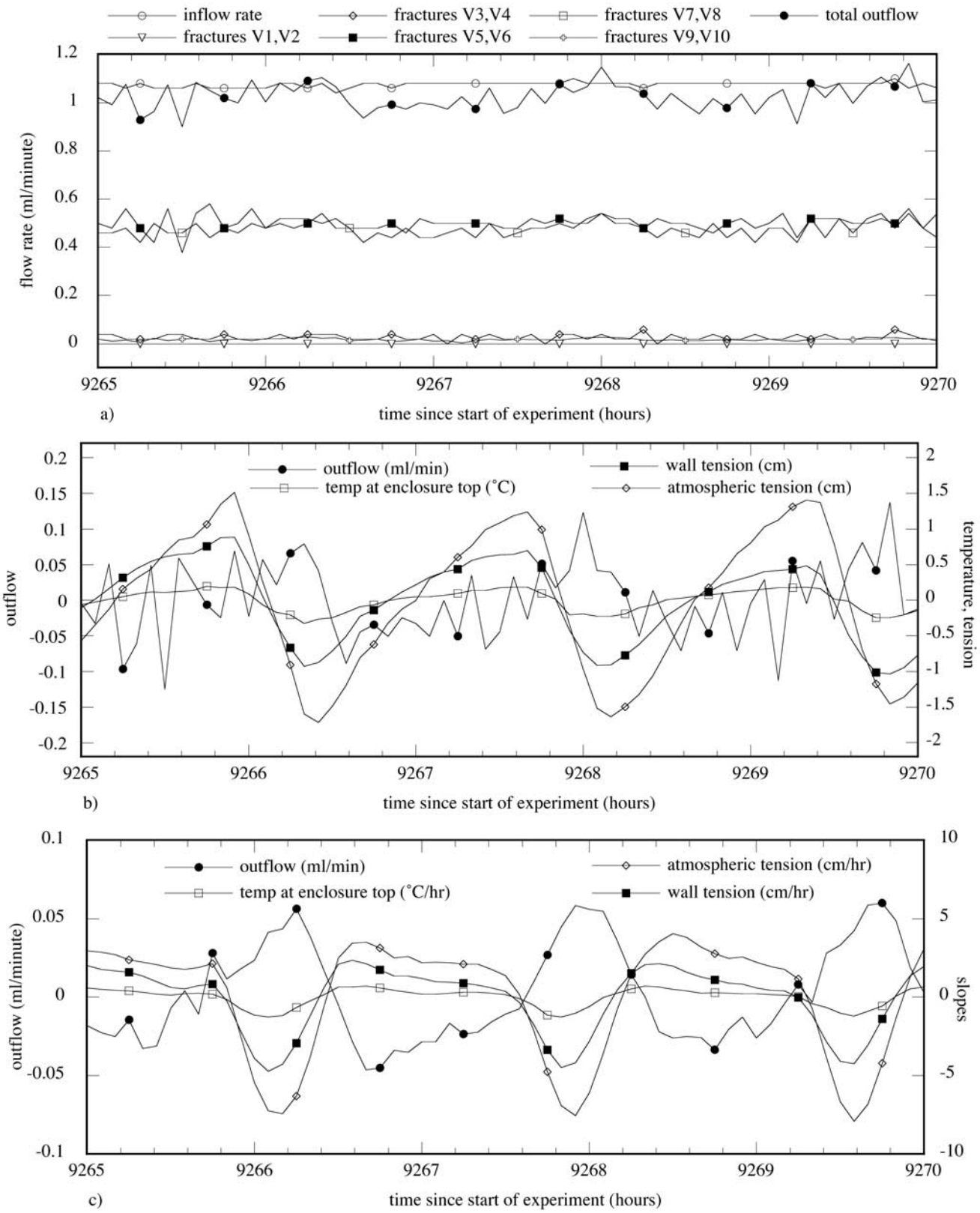

Figure 7. Outflow, temperature, vapor and liquid tension correlations for 5 hour period during temperature control: a) Expanded outflow rates. b) Fluctuations from the mean value for total outflow rate, temperature, vapor tension and liquid tension. Mean values of 1.025 ml/min, 22.86°C, 31.76 cm, and 2.305 cm, respectively. c) Correlations between rates of change for temperature, vapor tension and liquid tension and smoothed total outflow.

installation onward, while those at the far outsides displayed tensions of ~100 cm or above when installed, with a decline to ~60 cm or less by the end of the test. Therefore, despite a lack of visual evidence, bricks outside of the flow field apparently continued to wet (slow lateral flow and/or vapor transport) throughout the course of the experiment. Finally, many, but not all of the tensiometers showed unsteady responses much greater than the instrument error (~0.1 cm); oscillations of up to ~1 cm were observed in the wetted region near the middle of the wall, while oscillations of up to ~10 cm were observed in both the vapor tension, and in bricks away from the wetted plume.

[23] Thermocouple data showed that the temperature within the experiment ranged from lows of ~19°C during the winter to highs of ~23°C in the summer. This seasonal variation was overlain by generally smooth and nearly periodic (several hr to 24 hr) oscillations with maximum amplitudes of ~1°C. Considering short time behavior, we see that during the winter months, periodic oscillations below ~12 hours are mostly absent, while such oscillations are dominant during the spring to early summer, presumably due to the laboratory cooling system. We also found that on weekends during the spring to summer, the temperature control circuitry shut off, and laboratory temperature drifted slowly, with only a diurnal oscillation present. In all instances, temperature oscillations in the laboratory were sequentially dampened within the external enclosure by ~25% and inside the experimental enclosure by an additional ~25%. Finally, air temperature at the top of the brick wall was consistently ~0.7°C warmer than at the bottom.

[24] Data collected during the winter shows erratic outflow behavior (see Figures 5 and 6) with little to no correlation to tension or temperature. However, if we focus on the spring and summer period, the fact that our laboratory cooling system shut down during weekends allows us to understand a bit more about the nature of the short time fluctuations that occurred throughout our experiment. We illustrate this with a series of plots that cover two typical 5 hour acquisition periods, 9265–9270 hours at the end of a week (Figure 7) and 9320–9325 hours over the weekend (Figure 8). We see a periodic signal (~2 hours) in the total outflow rate when the temperature control is on (Figure 7a), while no periodicity is apparent when the temperature drifted on the weekend (Figure 8a). Despite the obvious difference in low frequency information, variance in the total outflow rate does not differ significantly between these two segments (0.00302 cm^2/min^2 for the control period and 0.00337 cm^2/min^2 for the drift period). In both plots, short wavelength variability in total outflow appears directly correlated to outflow from individual fracture pairs, mainly fracture 5–6 and 7–8 (less so). Figures 7b and 8b show fluctuations from the mean in the total outflow rate, temperature within the experimental enclosure, vapor tension, and liquid tension near the middle of the transect. Temporal correlations between the latter three are obvious during room control. However, during the weekend drift period, the two tension measurements slowly climb, but appear uncorrelated to the near constant temperature.

[25] To consider the tie between temperature, tension, and outflow, we plot the rate of change for the first two calculated using a five-point central difference in time and compare to smoothed outflow calculated with a comparable five-point moving average (Figures 7c and 8c). During controlled cooling, the maximum rates of change for temperature and tension line up closely, and maximum outflow lags only slightly. Warming periods show the reverse, but with slightly less temporal correspondence. Meanwhile, during the temperature drift period, outflow is uncorrelated to the slopes of either temperature or tension.

[26] We can explain behavior during the temperature control period with a simple evaporation-condensation mechanism. As temperature within the experimental enclosure drops, the balance between evaporation and condensation shifts toward condensation, with a maximum rate corresponding to the maximum rate of change in temperature. Liquid tensions within the bricks react immediately to the thermally induced condensation. Flow within the fracture–matrix network will also respond immediately, however, outflow appears slightly lagged because flow must move through the wick to be recorded on the balance. During the uncontrolled drift period, both vapor and matrix tension also drift, while temperature remains essentially constant; outflow continues to behave erratically, with fluctuations that are similar in magnitude to those measured during the controlled period. Thus, we conclude that fluctuations such as seen during the drift period occur spontaneously within the fracture–matrix network.

[27] The cause of the spontaneous fluctuations with our experiment is currently unknown, but likely due to some form of pulsation along flow pathways similar to that seen in two fractures of Experiment 1 where gravity-driven fingering was documented. It seems unlikely, however, that isolated dripping within individual fractures alone could yield excursions of above 20% in total and 50% in individual (5–6) outflow rates, thereby suggesting a system scale linkage of small-scale flow processes. Such a linkage is likely due to the influence of fracture intersections acting as capillary barriers. Finally, we note that the variances in total outflow for these periods at ~9300 hours (Figures 7 and 8) are greater than at ~1200 hours (Figure 5c) and over twice that at ~2600 hours (Figure 6). Thus, for no apparent reason, fluctuations that were damped on the implementation of humidity barrier around the experimental enclosure, have now increased in strength.

4.5. Long-Term Average Outflow–Inflow Trends (Entire Experiment)

[28] Data was acquired over discrete intervals that varied in length, but were generally 1, 2, or 3 days long. Following each data acquisition period, data was downloaded and the experiment serviced if necessary, leading to a normal down time of one to four hours. There were also a number of short periods (~1–2 days in length) when data was either lost or obviously incorrect (malfunction or human error). Additionally, there are three long periods where data was not acquired: from ~1600 to 2500 hours (first set of system modifications), from ~8000 to 9000 hours (we had time only to maintain the experiment), and from ~10,100 to 10,500 hours (we turned the inflow off). To consider variations in the contribution to the total outflow from individual fracture pairs throughout the course of the experiment, we average the inflow rate and outflow rates for each

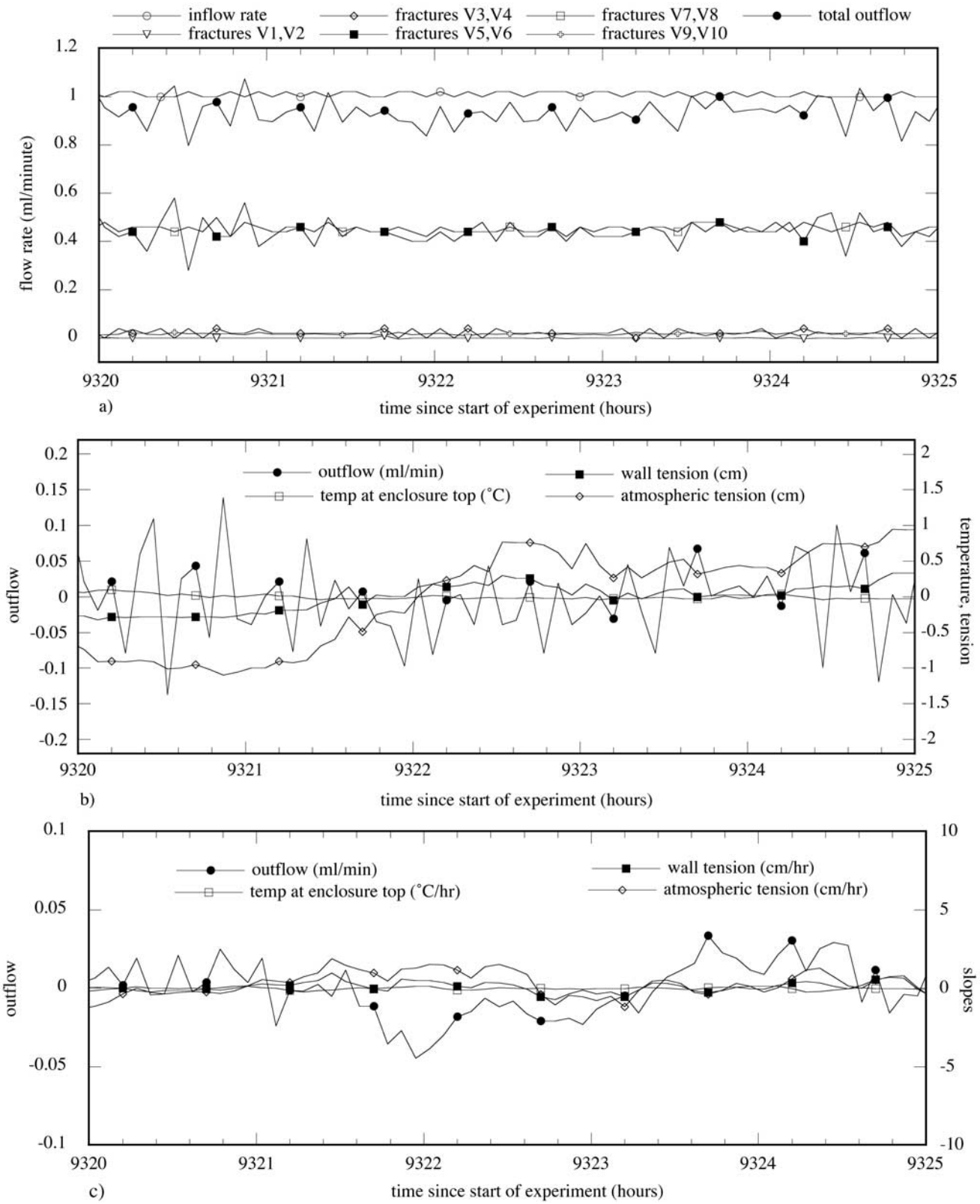

Figure 8. Outflow, temperature, vapor and liquid tension correlations for 5 hour drift period: a) Expanded outflow rates. b) Fluctuations from the mean value for total outflow rate, temperature, vapor tension and liquid tension. Mean values of 0.935 ml/min, 22.34°C, 26.63 cm, and 4.030 cm, respectively. c) Correlations between rates of change for temperature, vapor tension and liquid tension and smoothed total outflow.

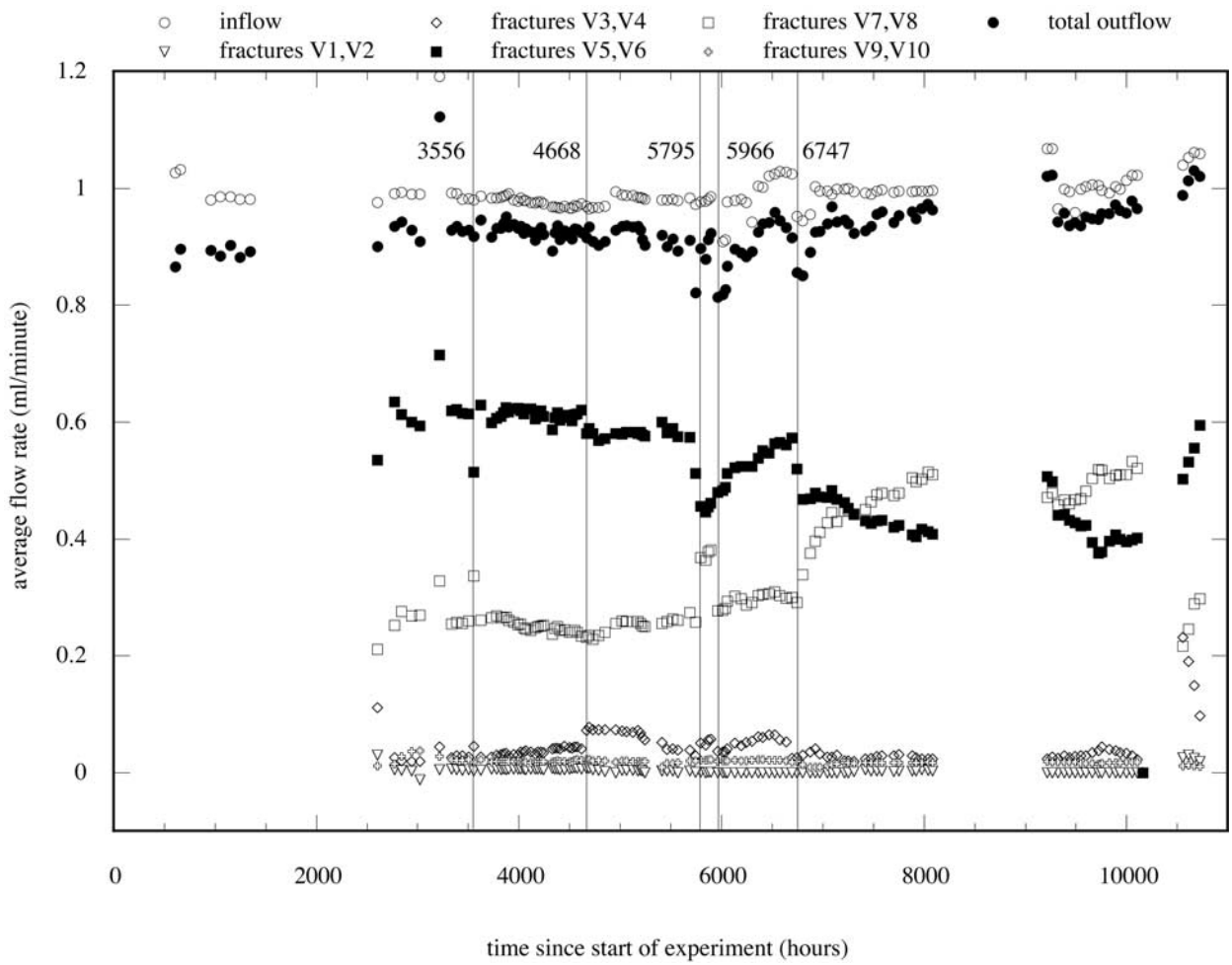

Figure 9. Average inflow and outflow rates over the course of Experiment 2: 5 minute data have been averaged for each acquisition period (1–3 days) throughout the experiment. Data were not acquired from ~1600 to 2500 hours (first set of system modifications), from ~8000 to 9000 hours (we had time only to maintain the experiment), and from ~10,100 to 10,500 hours (we turned the inflow off and then back on). Obvious pathway switches have been identified with vertical lines at 5 times (3556, 4668, 5795, 5966, 6747 hours).

over the span of an individual data acquisition period (Figure 9).

[29] In general, the average total outflow shows more variability than the average imposed inflow. Individual outflow rates show an even greater amount of variation, with the relative contributions of fractures 5–6 crossing 7–8 two times during the course of the experiment. We also see clear evidence of pathway "switching" behavior at least five times (at 3556, 4668, 5795, 5966, 6747 hours), all of similar magnitude to that found within individual data sets (e.g., Figure 6). For three of these switches, we can identify correlated external perturbations. During the period before 5795 hours, we worked on the experimental enclosure to install holes for tensiometer tubes; subsequently, flow from 5–6 goes down while 7–8 goes up. At 5966 hours, an ~9% decrease in inflow rate during the preceding 24 hours triggered 3–4 and 7–8 to decrease while 5–6 increases. System level changes triggered by inflow also occur at 6747 hours. There, inflow (1.03 ml/min) was over adjusted downward (0.95 ml/min) causing 5–6 to decrease. Then when inflow is adjusted up to 1.0, 7–8 increases in outflow while 5–6 remains constant. While these three instances demonstrate that inflow changes or evaporation events can trigger a system change, many other instances of such perturbations yielded little or no response in the average outflows, or the relative contributions of different pathways. As a notable example, the pump was accidentally disturbed at 3335 hours, causing inflow to increase by ~20%, with corresponding increased outflow from most of the fracture pairs. However, after readjusting the inflow, all outflows returned to their preperturbed values.

[30] At ~10,100 hours, we turned inflow off and then turned it back on at ~10,500 hours. Outflow began after ~5 hours, and rose to an average preturnoff outflow rate after ~20 hours. Average outflow rates for the four subsequent data acquisition periods are shown as the final four points on Figure 9. The behavior of fractures 3–4 is quite interesting, as they had not participated much before the inflow interruption, and yet contributed strongly to total outflow shortly after inflow began. The relative contribu-

tions of the fracture sets continued to vary with 5–6 and 7–8 increasing at the expense of 3–4 until the experiment was terminated at 10,795 hours.

[31] Although total outflow occasionally exceeded inflow for an individual measurement (see Figures 7a and 8a), average inflow always exceeded average outflow (Figure 9). This discrepancy between average inflow and outflow is much greater than what can be accounted for by the continued wetting of the bricks outside the core of the diffuse plume. Instead, it is a measure of the intensity of the ongoing vapor phase transport and evaporation-condensation mechanisms that occurred within the experimental system. Because water condensed on the internal surface of the experimental enclosure (running down and pooling at the bottom where it subsequently leaked slowly underneath), such a discrepancy would have continued indefinitely and precluded calculation of the average moisture content within the brick wall.

5. Summary of Principal Observations

[32] We summarize our experimental results in a series of *Principal Observations*. Both experiments behaved in a similar manner during the initial stages of wetted structure development; principle observations from this early time are presented in section 5.1. At later time (i.e., after the fracture–matrix networks were spanned from top to bottom), the two experiments evolved differently; principal observations from Experiment 1 where evaporation and mineral precipitation processes dominated are presented in section 5.2, while those from Experiment 2 where these same processes were minimized are presented in section 5.3. We note that while *Observations 7–9* were derived from Experiment 2 where evaporation and mineral precipitation processes were minimized, they likely apply to Experiment 1 as well.

5.1. Early Time (Experiments 1 and 2)

[33] 1) *Flow pathways evolved that remained primarily within the fractures with indications of gravity-driven fingering and associated pulsation*: Our fracture–matrix networks were designed to have tight fractures and a matrix with both significant storage capacity and capillary gradient (high porosity, initially dry, and small pores). Yet pathways formed primarily in the fractures, with less contribution through the matrix. Matrix flow along the pathways was presumably due to either the local tightening (lowered permeability) or loosening (capillary barrier) of the fracture network, and/or variability in the properties of the bricks across the network. When in the fractures, flow was predominantly gravity-driven, with obvious indications of gravity-driven fingering and associated pulsation in Experiment 1.

[34] 2) *Fracture intersections often behaved as capillary barriers that forced pathway shifts and generated multiple pathways*: Within the fracture network, fracture intersections acting as capillary barriers played a critical role in structural evolution. Downward flow within a fracture sometimes crossed an intersection, and sometimes turned 90 degrees, offsetting the flow path. In both experiments, such offsets led to the subsequent formation of secondary pathways originating at the intersection.

[35] 3) *Lateral interaction across fractures was minimal despite a system designed to assure physical contact*: Vertical fractures acted as capillary barriers, imparting a blocky nature to the development of the wetted structure. Bricks on either side of a flowing fracture wetted, however, lateral movement of the wetting front was restricted when it reached the next fracture. In the context of the entire fracture–matrix network, this behavior led to a wetted plume that was elongated in the direction of gravity.

5.2. With Active Evaporation and Mineral Precipitation Processes (Experiment 1)

[36] 4) *Evaporation limited the width of the wetted structure*: In Experiment 1, the primary pathway spanned the network in two days, then did not widen significantly in the next 7 days. The secondary pathway showed similar growth structure, but in "slow motion". By day 9, the composite plume looked somewhat parabolic; however, wetted structure at the bottom of the network provided clear evidence of discrete pathways within the plume.

[37] 5) *Evaporation-precipitation processes caused both strengthening and starvation of preferential pathways*: Evaporation of matrix equilibrated fluid and subsequent precipitation of calcium carbonate in Experiment 1 led to a gradual change in the flow field: extent of the flow field decreased, the primary pathway became starved of fluid, and all flow shifted into the secondary pathway with outflow at the bottom of the network retracted to a single fracture. On subsequent reduction of evaporation, the wetted structure swelled and two additional "tertiary" pathways formed, one of which was eventually starved, while the other was still growing at the end of the test.

5.3. With Minimized Evaporation and Mineral Precipitation Processes (Experiment 2)

[38] 6) *With minimal evaporation, wetted structure at long time took on the appearance of a diffuse plume*: In Experiment 2, slow lateral flow and vapor transport caused wetted structure within the fracture–matrix network to slowly evolve toward what appeared to be a diffuse plume. However, visual data is primarily a view of the matrix (as well as being only qualitative), and therefore is not an indicator of flow through the fracture–matrix network, in particular, the fractures. Within fractures, unsteady flow clearly continued (see *Observations 7, 8, and 9*, below).

[39] 7) *Pathways remained dynamic and continued to shift at all timescales within a relatively quiet environment and with steady inflow*: We found pathway shifts to occur throughout the 15 month duration of Experiment 2. Some of these were rapid "switches", while others were very gradual. Some rapid switches could be correlated with identifiable, but mild perturbations, some not. Near the end of the experiment a major perturbation was induced by interrupting the fluid supply for 16 days; pathways changed when flow was subsequently restarted.

[40] 8) *Slight temperature forcing imposed some unsteady behavior at timescales on the order of hours via a rapid evaporation-condensation mechanism*: Slight temperature forcing ($\sim$0.25°C) occasionally imposed by our laboratory heating and cooling system caused an evaporation-condensation mechanism that superimposed an unsteady signal on outflow. It is likely that diurnal temperature variations also imposed a similar process during the

initial period of the test before being significantly damped by the outer enclosure.

[41] 9) *System generated fluctuations in flow along individual pathways occurred at short times throughout the course of the experiment*: Outflow rates from the fracture–matrix network showed maximum fluctuations of over 20% in total outflow, and one of the fracture pairs showed maximum fluctuations of over 50%. Of particular interest is that while temperature swings forced a response in outflow (*Observation 8*), they did not remove or diminish the ever present fluctuations. The mechanism responsible for this short time dynamic behavior is currently unknown, but likely due to a system-scale pulsation mechanism analogous to that observed for gravity-driven fingers within individual fractures.

6. Discussion

[42] In retrospect, most of our results could have been deduced from current understanding of single fracture and single fracture–matrix processes, and many were hypothesized in some manner by *Glass et al.* [1995, 1996]. They suggested that fundamental flow processes within individual fractures and at fracture intersections could combine to generate large scale preferential flow through fracture networks, without a need to invoke system scale heterogeneity (e.g., faults). They went on to suggest that geochemical activity could act to either reinforce or extinguish such pathways. Here, we find that preferential flow pathways can indeed evolve within the fracture network, even in the presence of strong capillary forces associated with a highly porous matrix. Furthermore, Experiment 1 clearly demonstrated the potential for geochemical activity to influence the development of such pathways. However, in contrast to the conceptualization suggested by *Glass et al.* [1995, 1996], multiple pathways formed in each experiment, even though flow at the top of the fracture–matrix network initiated from a single fracture. Additionally, we found fluctuation at a variety of timescales that incorporated temporal variation along individual pathways, as well as switching between. We further discuss these discoveries and their linkage below.

[43] The development of the initial wetted structure showed that the formation of secondary pathways occurred at flow offsets associated with fracture intersections. This observation is similar to what has been found in unstable flow fields within both individual fractures [*Nicholl et al.*, 1993] and sands [*Glass et al.*, 1989] where slow growing dendrites initiate from appendages along gravity-driven fingers under steady supply. Multiple pathway formation has also been documented in gravity destabilized nonwetting invasion experiments within fractures [*Glass and Nicholl*, 1995] and heterogeneous sands [*Glass et al.*, 2000] where it was associated with locations of pulsation. Pulsation was indeed documented within two vertical fractures in Experiment 1, and used as our designator for the occurrence of gravity-driven fingering. However, to obtain pathway switching, pulsation must occur at fracture intersections where pathway choices are made. In addition, the size or volume of the pulse must be increased along with a decrease in its frequency to yield behavior similar to that seen in the outflow of Experiment 2. A larger volume acting at lower frequency could arise from an integrator, or through a cascade process at a critical state, or both. Such mechanisms are unlikely within the single small fractures contained within our experiment and therefore must arise as an attribute of the fracture network. Thus, we suggest the influence and behavior of fracture intersections as well as their connection to be very important.

[44] Fracture intersections are likely to form a network within the fracture network with possible behavior that could range from barriers and flow integrators/switches to conduits for preferential flow. Let us consider the simplest possible geometry for a fracture intersection of a junction between two sets of perpendicular parallel plates, much like those in our current experiment. Such an intersection will have a larger opening than either fracture, and thus will form a barrier to the wetting phase for low flows where tensions are high. Functioning as capillary barriers, such intersections will work to both concentrate flow at the scale of an individual fracture (i.e., cause the confluence of gravity-driven fingers above an intersection), and fragment flow into discrete pathways at the network scale (i.e., break lateral connection via vertical barriers). Additionally, barriers will likely behave as hysteretic gates, integrating flow from above until the intersection is breached, and then remaining open to pass the integrated volume before once again closing. As fluid passes the barrier, competition between capillary, gravitational, viscous, and possibly inertial forces will cause it to choose one of the three possible pathways, thereby allowing for switching. Finally, if we consider higher flow conditions where pressures are greater, such simple intersection geometry may reverse roles to provide connected high flow pathways through the network. Of course, this simple example is just one of the myriad of possibilities that must be considered and studied.

[45] Finally, we note that within a fracture–matrix network, several recent experiments conducted in the field have also shown temporal and some spatial dynamics suggestive of unsteady behavior even under reasonably long-term steady supply conditions [e.g., *Dahan et al.*, 1999; *Faybishenko et al.*, 2000; *Podgorney et al.*, 2000]. Such behavior is consistent in a general sense with what we have found in our mesoscale experiments within a controlled laboratory setting. In addition to system imposed fluctuations, one would expect that natural fracture–matrix networks will be subject to temperature forcing that could drive evaporation-condensation mechanisms such as we observed in the laboratory. Of course, the natural system will be exposed to spatially dependent temperature fluctuations that range widely in frequency and amplitude. In addition, we emphasize that the constancy of the fracture network and its physical and chemical properties cannot in general be taken for granted, especially in the field. With small changes in the local stress field, critical pathways for growth or flow may be interrupted as the fracture network and, in particular, intersections adjust. There is also evidence that within networks, fracture coatings and the erosion and mobilization of fillings can create situations where the physical and chemical domain of the network may be changing in time [e.g., *Weisbrod et al.*, 1999]. Additionally, ever present microbial activity can lead to the formation of biofilms that may clog or alter pathways [e.g., *Brown et al.*, 1994] as well as a time varying release of

surface active chemicals [e.g., *Totsche et al.*, 1997]. In combination with boundary conditions often driven by weather, flow within unsaturated, fractured rock remains a topic of considerable uncertainty.

7. Concluding Remarks

[46] Results from our mesoscale experiments in an unsaturated fracture–matrix network demonstrate the development of discrete flow pathways that are heavily controlled by processes acting within the fracture network, emphasizing the dual roles of fractures as both flow conductors and capillary barriers. Evaporation and the associated mineral precipitation were shown to significantly influence system behavior following development of the initial wetted structure. When evaporation-precipitation processes were important (Experiment 1), behavior ensued that included: pathway starvation and shifting, flow field narrowing/constraining, and the development of tertiary pathways when evaporation was somewhat reduced. When evaporation-precipitation processes were minimized (Experiment 2), the wetted structure eventually attained a visually diffuse plume. However, outflow measurements from this visually diffuse structure showed flow to be far from uniform or steady; throughout the course of this 15 month experiment, flow switched between various discrete pathways, and on timescales of minutes to hours, fluctuations in outflow rate were ever present. While some of these fluctuations can be associated with a temperature forced evaporation-condensation mechanism, others appear to arise naturally within the system from internal flow processes. We suggest that fracture intersections play a critical role in this regard as well as in causing pathway switching. Taken together, the results from both experiments demonstrate that even under conditions of constant supply, unsaturated flow through fractured rock will create discrete pathways and, in time, these pathways will be dynamic, both moving in space and imparting fluctuations to the outflow.

[47] Our experiments were designed as a first step in the study of how processes within single-fractures and single fracture–matrix blocks combine to determine behavior within a fracture–matrix network. We considered only a single, regular network of tight fractures within a matrix where capillary forces would be significant. In nature, fracture networks are highly variable in terms of both connection and topology. Furthermore, properties of the intervening matrix will range the full spectrum from highly sorptive sandstones to nearly impermeable granites. A full consideration of unsaturated flow though fractured rock masses that spans reality will require significant experimentation and the development of new conceptual models. However, we expect the behavior demonstrated in our experiments to persist in parameter space and increase in strength as we move toward a less permeable rock matrix in combination with wider fractures such as can be found in formations of welded tuff (e.g., Yucca Mountain Site) or basalt (e.g., Idaho National Engineering and Environmental Laboratory Site). In such unsaturated fractured rock masses, the implications of discrete pathway formation and subsequent spatial/temporal dynamics can be considerable for both the modeling and monitoring of contaminant transport.

[48] **Acknowledgments.** These experiments were conducted in 1995–1997 at the Flow Visualization and Processes Laboratory, Sandia National Laboratories, with support from the U.S. Department of Energy's Basic Energy Sciences Geoscience Research Program under contract DE-AC04-94AL85000. The analysis of experimental results and the writing of this manuscript was supported by the Idaho National Engineering and Environmental Laboratory, operated for the U.S. Department of Energy under contract DE-AC07-99ID13727. The authors wish to thank Justin von Deming, Lee Orear, Nick Tetsi, Don Fox, Stephanie Pankretz, Vince Tidwell, and David Lopez for their efforts in constructing and maintaining the experiments and Kristine Baker for the measurement of brick matrix properties.

References

Brown, D. A., D. C. Kamineni, J. A. Sawicki, and T. J. Beveridge, Minerals associated with biofilms occurring on exposed rock in a granitic underground research laboratory, *Appl. Environ. Microbiol.*, *60*, 3182–3191, 1994.

Conca, J. L., and J. Wright, *Procedures for Using the UFA to Measure the Matric Potential of Core Samples*, *UFA Method Tech. Procedures*, UFA Ventures, Inc., Richland, Wash., 1997.

Dahan, O., R. Nativ, M. Adar, B. Berkowitz, and Z. Ronen, Field observation of flow in a fracture intersecting unsaturated chalk, *Water Resour. Res.*, *35*(11), 3315–3326, 1999.

Davidson, G. R., R. L. Bassett, E. L. Hardin, and D. L. Thompson, Geochemical evidence of preferential flow of water through fractures in unsaturated tuff, Apache Leap, Arizona, *Appl. Geochem.*, *13*(2), 185–195, 1998.

Fabryka-Martin, J. T., P. R. Dixon, S. S. Levy, B. Liu, D. L. Brenner, L. E. Wolfsberg, H. J. Turin, and P. Sharma, Implications of environmental isotopes for flow and transport in the unsaturated zone at Yucca Mountain, Nevada, 1996 Annual Meeting of the Geological Society of America, October 28–31, Denver, CO, GSA abstracts with programs, vol. 28(7), A-416, 1996.

Faybishenko, B., C. Doughty, S. Steiger, J. Long, T. Wood, J. Jacobsen, J. Lore, and P. Zawislanski, Conceptual model of the geometry and physics of water flow in a fractured basalt vadose zone, *Water Resour. Res.*, *36*(12), 3499–3520, 2000.

Glass, R. J., and M. J. Nicholl, Near drift two-phase flow processes within regionally saturated fractured rock, in *Proceedings of the 6th International Conference on High Level Radiation and Waste Management*, 30 April–5 May, pp. 212–216, Am. Nucl. Soc., Las Vegas, Nev., 1995.

Glass, R. J., and M. J. Nicholl, Physics of gravity driven fingering of immiscible fluids within porous media: An overview of current understanding and selected complicating factors, *Geoderma*, *70*, 133–163, 1996.

Glass, R. J., T. S. Steenhuis, and J.-Y. Parlange, Mechanism for finger persistence in homogeneous unsaturated porous media: Theory and verification, *Soil Sci.*, *148*, 60–70, 1989.

Glass, R. J., M. J. Nicholl, and V. C. Tidwell, Challenging models for flow in unsaturated, fractured rock through exploration of small scale flow processes, *Geophys. Res. Lett.*, *22*(11), 1457–1460, 1995.

Glass, R. J., M. J. Nicholl, and V. C. Tidwell, Challenging and improving conceptual models for isothermal flow in unsaturated, fractured rock through exploration of small scale processes, SAND95-1824, 61 pp., Sandia National Laboratories, Albuquerque, N. M., 1996.

Glass, R. J., S. H. Conrad, and W. Peplinski, Gravity destabilized nonwetting phase invasion in macroheterogneous porous media: Experimental observations of invasion dynamics and scale analysis, *Water Res. Res.*, *36*(11), 3121–3137, 2000.

Glass, R. J., H. Rajaram, M. J. Nicholl, and R. L. Detwiler, The interaction of two fluid phases in fractured media, invited paper, *Curr. Opin. Colloid Interface Sci.*, *6*, 223–235, 2001.

Glass, R. J., M. J. Nicholl, A. L. Ramirez, and W. D. Daily, Liquid phase structure within an unsaturated fracture network beneath a surface infiltration event: Field experiment, *Water Resour. Res.*, *38*(10), 1199, doi:10.1029/2000WR000167, 2002.

Nicholl, M. J., R. J. Glass, and H. A. Nguyen, Small-scale behavior of single gravity-driven fingers in an initially dry fracture, in *Proceedings of the Fourth Annual International Conference on High Level Radiation and Waste Management*, 26–30 April, pp. 2023–2032, Am. Nucl. Soc., Las Vegas, Nev., 1993.

Podgorney, R. K., T. R. Wood, B. Faybishenko, and T. M. Stoops, Spatial and temporal instabilities in water flow through variably saturated fractured basalt on the one-meter field scale, in *Dynamics of Fluids in Frac-*

tured Rock, *Geophys. Monogr. 122*, pp. 129–146, AGU, Washington, D. C., 2000.

Russell, C. E., J. W. Hess, and S. W. Tyler, Hydrogeologic investigation of flow in fractured tuffs, Rainier Mesa, Nevada Test Site, in *Flow and Transport Through Unsaturated Fractured Rock*, *Geophys. Monogr. 42*, edited by D. D. Evans and T. J. Nicholson, pp. 43–50, AGU, Washington, D. C., 1987.

Su, G. W., J. T. Geller, K. Pruess, and F. Wen, Experimental studies of water seepage and intermittent flow in unsaturated, rough-walled fractures, *Water Resour. Res.*, *35*(4), 1019–1037, 1999.

Totsche, K. U., J. Danzer, and I. Kogel-Knabner, DOM-enhanced retention of polycyclic aromatic hydrocarbons in soil miscible displacement experiments, *J. Environ. Qual.*, *26*(4), 1090–1100, 1997.

Weisbrod, N., R. Nativ, E. Adar, and D. Ronen, Impact of intermittent rainwater and wastewater flow on coated and uncoated fractures in chalk, *Water Resour. Res.*, *35*(11), 3211–3222, 1999.

R. J. Glass and S. E. Pringle, Flow Visualization and Processes Laboratory, Geohydrology Department, Sandia National Laboratories, Mail Stop 0735, Albuquerque, NM 87185-0735, USA. (rjglass@sandia.gov)

M. J. Nicholl, Department of Materials, Metallurgical, Mining, and Geological Engineering, University of Idaho, Moscow, ID 83843, USA.

T. R. Wood, Idaho National Engineering and Environmental Laboratory, Idaho Falls, ID 83415, USA.